NANO LETTERS

Letter

High-Throughput Fabrication of Resonant Metamaterials with Ultrasmall Coaxial Apertures via Atomic Layer Lithography

Daehan Yoo,[†] Ngoc-Cuong Nguyen,[‡] Luis Martin-Moreno,[§] Daniel A. Mohr,[†] Sol Carretero-Palacios,[∥] Jonah Shaver,[†] Jaime Peraire,[‡] Thomas W. Ebbesen,[⊥] and Sang-Hyun Oh[*,†]

[†]Department of Electrical and Computer Engineering, University of Minnesota, Minneapolis, Minnesota 55455, United States

[‡]Department of Aeronautics and Astronautics, Massachusetts Institute of Technology, Cambridge, Massachusetts 02139, United States

[§]Instituto de Ciencia de Materiales de Aragón and Departamento de Física de la Materia Condensada, CSIC-Universidad de Zaragoza, E-50009 Zaragoza, Spain
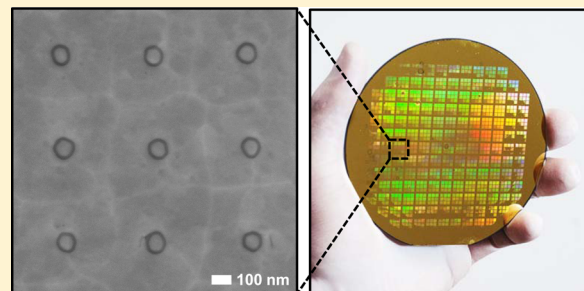
[∥]Instituto de Ciencia de Materiales de Sevilla, CSIC-Universidad de Sevilla, 41092 Sevilla, Spain

[⊥]ISIS, University of Strasbourg and CNRS, 67000 Strasbourg, France

Ⓢ Supporting Information

ABSTRACT: We combine atomic layer lithography and glancing-angle ion polishing to create wafer-scale metamaterials composed of dense arrays of ultrasmall coaxial nanocavities in gold films. This new fabrication scheme makes it possible to shrink the diameter and increase the packing density of 2 nm-gap coaxial resonators, an extreme subwavelength structure first manufactured via atomic layer lithography, both by a factor of 100 with respect to previous studies. We demonstrate that the nonpropagating zeroth-order Fabry-Pérot mode, which possesses slow light-like properties at the cutoff resonance, traps infrared light inside 2 nm gaps (gap volume $\sim \lambda^3/10^6$). Notably, the annular gaps cover only 3% or less of the metal surface, while open-area normalized transmission is as high as 1700% at the epsilon-near-zero (ENZ) condition. The resulting energy accumulation alongside extraordinary optical transmission can benefit applications in nonlinear optics, optical trapping, and surface-enhanced spectroscopies. Furthermore, because the resonance wavelength is independent of the cavity length and dramatically red shifts as the gap size is reduced, large-area arrays can be constructed with $\lambda_{\text{resonance}} \gg$ period, making this fabrication method ideal for manufacturing resonant metamaterials.

KEYWORDS: Coaxial nanohole, atomic layer lithography, glancing-angle ion milling, slow light, extraordinary optical transmission, epsilon-near-zero metamaterial

Engineered metallic apertures and resonant cavities that confine light into nanometric volumes are powerful tools for plasmonics, biochemical sensing, imaging, optical trapping, nonlinear optics, and nanophotonics.[1−6] Coaxial nanoapertures[7−12] have been of particular interest in this area due in part to their unique properties arising from the zeroth-order Fabry-Pérot (FP0) mode, which occurs spectrally close to the cutoff frequency of the TE_{11} waveguide mode. At this cutoff resonance, the propagation constant approaches zero, resulting in a model epsilon-near-zero (ENZ) material.[13,14] As the phase velocity diverges and the group velocity is greatly diminished, extreme, uniform field enhancement is enabled by a "slow light" effect caused by the trapping of light inside the aperture as well as other intriguing effects such as supercoupling and squeezing of light into ultranarrow waveguides, and transmission that is nearly independent of the channel length.[15] Because a normally incident plane wave is efficiently coupled to this resonant mode, extraordinary optical transmission (EOT)[1] can readily be observed.

In this coaxial metal–insulator–metal (MIM) geometry, the cutoff wavelength is governed by the gap size and diameter of the annular aperture.[12] The highly tunable cutoff resonance available in this geometry can couple and store a significant amount of optical energy into ultracompact ring-shaped nanocavities. However, the reproducible, high-throughput fabrication of compact coaxial structures, in particular with single-digit-nanometer gaps, has been very challenging. Optical interference lithography was used to produce coaxial aperture arrays but only with gap sizes of larger than 60 nm.[16,17] Focused ion beam milling[10,18] can create narrow gaps but only over small areas and the gap width is nonuniform throughout the film thickness due to metal redeposition. Our previous work[19,20] addressed the challenge of mass-producing long and uniform annular gaps down to 1 nm in width but was limited by
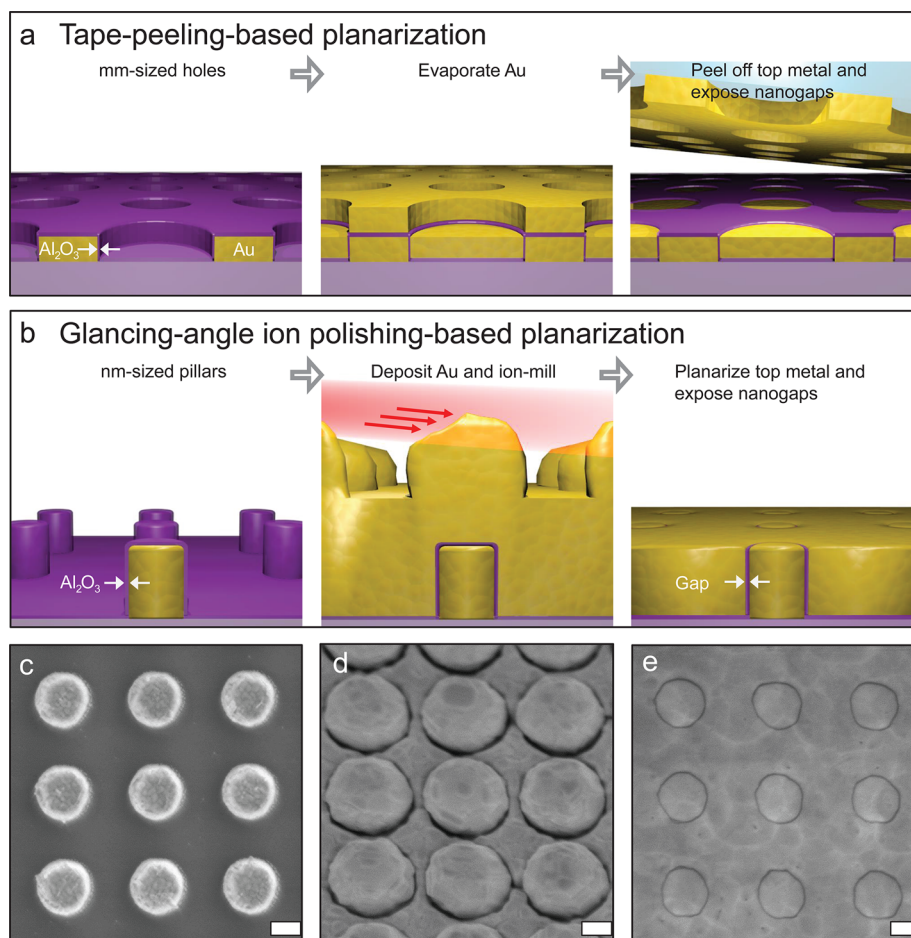
Figure 1. (a) Schematic flow of the tape-peeling-based nanogap fabrication. (b) Schematic flow of our new fabrication process used for the coaxial nanocavity array using glancing-angle ion polishing. (c) First, the Au pillar arrays are patterned on a sapphire wafer using e-beam lithography, metal evaporation, and lift-off. An ALD Al_2O_3 film is then conformally coated on the patterned Au pillar array. The array periodicity is 500 nm, and the pillar diameter is 250 nm. (d) Second Au film is conformally deposited atop of the Au pillar array and then selectively etched away through glancing-angle ion polishing. (e) Patterned Au surface is planarized by glancing-angle ion polishing, which exposes vertically oriented Al_2O_3 gaps. Scale bars: (c−e) 150 nm.

photolithography and our tape-peeling method in resonator diameter and array periodicity, leading to terahertz regime FP0-mediated enhanced transmission. In order to maintain the 1−2 nm gap sizes required for extreme field enhancements and enable operation at visible and infrared (IR) frequencies, the diameter of the coaxial resonator must be reduced by ∼100 fold.

In this work, we overcome this miniaturization challenge for atomic layer lithography and construct ultracompact, high-aspect-ratio coaxial nanocavities with gaps as small as 2 nm and diameters as small as 100 nm. These structures exhibit higher order resonances at frequencies as high as the optical and FP0 resonances in the near-infrared (NIR), representing an improvement of 2 orders of magnitude with respect to our previous work. Using a dense array of these nanocavities, we measure EOT mediated by cutoff resonances through gaps as narrow as 2 nm, revealing ENZ-like properties, efficient coupling and channel-length-independent resonance, arising from the FP0 mode. Our experiments combine atomic layer lithography, which turns atomic layer deposition (ALD)[21,22] into an angstrom-resolution gap-forming method,[19] with a wafer-scale glancing-angle ion polishing technique. The combination of these two powerful methods can create ultrasmall coaxial nanocavities at extreme densities over an entire wafer, opening up the door to devices with sub-10 nm gaps and FP0 resonances in the NIR and potentially even in the visible. High-density packing of coaxial nanocavities, combined with an ultrasmall gap size, leads to extreme nanoscale light confinement, field enhancements, and transmission efficiency. This method allows for large-area patterning, efficient light coupling, and emission at normal incidence and confinement of "slow" light alongside the nanogap ring near the cutoff condition. These properties can be harnessed for nonlinear optics,[23,24] metamaterials,[25,26] light trapping,[27,28] coaxial nano-lasers,[29] particle trapping,[30] and spontaneous emission enhancement.[31]

As shown in Figure 1, atomic layer lithography, which we define as a fabrication scheme to control critical gap dimensions using ALD, can be implemented via different approaches to planarize and expose vertical nanogap structures. Our previous work[20] demonstrated the unique possibility of fabricating arrays containing very long nanogap loops (perimeter of up to ∼1 cm) as illustrated in Figure 1a. To push FP0 resonances to the NIR and visible, the diameter of each coaxial gap should be in the deep-submicron regime. The critical challenge in making high-aspect-ratio coaxial nanowaveguides via tape-peeling-based nanogap fabrication is filling the submicron core region with metals. To solve this problem, we invert the process sequence
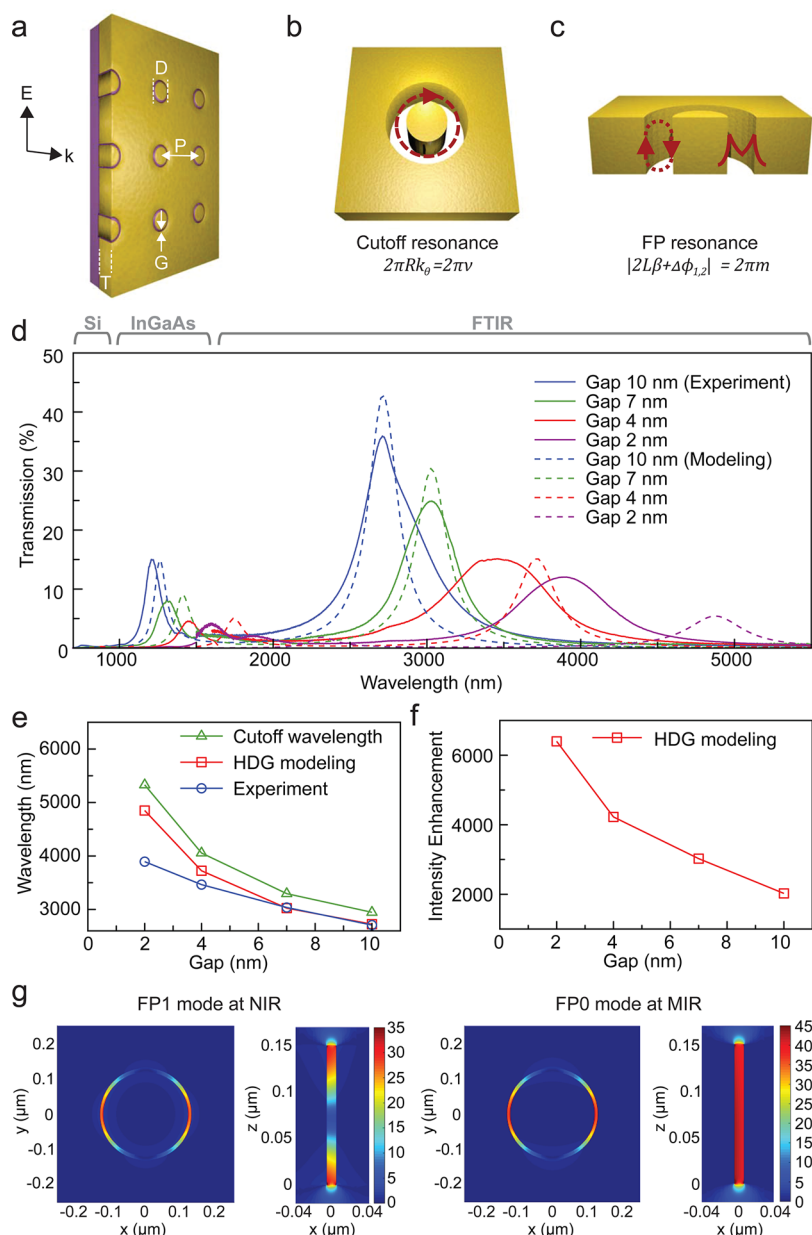
Figure 2. Extraordinary transmission through the coaxial aperture array. (a) Schematic of a coaxial aperture array. Illumination is through a sapphire substrate with unpolarized light, and transmission spectrum is measured using three different spectroscopic systems covering over three full octaves from 400 to 5000 nm in wavelength. (b,c) Schematics of coaxial waveguides with the cutoff resonance and the FP resonance. (d) Measured and simulated spectra of light transmitted from the coaxial aperture array with a 250 nm diameter and four different gap widths (2, 4, 7, 10 nm). (e) Variation of transmission peak wavelength of the FP0 ($m = 0$) resonance as a function of gap width in the coaxial aperture array. (f) Intensity enhancement for the FP0 resonance as a function of gap width. (g) Calculated electric field distributions of 250 nm diameter coaxial aperture with a 10 nm gap at the resonance wavelengths of 1200 and 2700 nm.

by first forming high-aspect-ratio metal pillars, that is, the core region, followed by ALD coating to define the gap size and then a conformal metal cladding deposition. After this step, the entrance of coaxial nanocavities is exposed by glancing-angle ion polishing to shave off residual metals on the surface (Figure 1b). Tape-peeling-based planarization is suitable for manufacturing large nanogap loops (from tens of micrometers to a few centimeters in perimeter), whereas glancing-angle ion polishing is optimized for large-area submicron coaxial nanoaperture arrays.

Our new fabrication method is illustrated in Figure 1b with corresponding scanning electron micrographs (SEMs in Figure 1c−e). In this exemplary structure, first, a square array of 200

nm tall gold pillars (diameter, 250 nm; period, 500 nm; array size, 200 μm × 200 μm) is patterned on a sapphire substrate using electron-beam lithography. For large-area fabrication after optimal parameters are chosen, nanoimprint or photolithography can be used. Next, the critical dimension (gap width) is defined via an ALD-grown alumina (Al_2O_3) film, which conformally covers the exposed gold surfaces (Figure 1c). A second layer of gold (400 nm) is then deposited to form the metal−insulator−metal (MIM) structures (Figure 1d). Finally, the top surface is planarized via glancing-angle ion milling (10° from surface) to expose the Al_2O_3-filled coaxial apertures. During this process, the bumps in the second gold layer are shaved off by Ar ion bombardment whereas flat regions are

shadowed and protected. As the planarization process continues, this shadowing effect gradually dissipates, and the entire film is polished uniformly. A top view SEM (Figure 1e) shows an array of coaxial apertures with a 250 nm diameter and 10 nm Al_2O_3 gap formed through the entire thickness of a 150 nm gold film. The sample before planarization by glancing-angle ion milling shows a height difference of 200 nm (Figure S1), which corresponds to the core metal thickness. After ion milling, the height difference was reduced to below 20 nm, as confirmed by atomic force microscopy (AFM) (Figure S1). In this process, the flatness after polishing is controlled by the incidence angle of the ion beam. Using an ion beam with a glancing angle lower than 10° can further reduce the height difference. Because ductile metals such as gold are not amenable to standard polishing methods, this new technique could also find applications in eliminating topographic variations in other metallic nanostructures.

The geometry of the coaxial nanocavity array is determined by the metal film thickness (T), inner diameter of the annular gap (D), gap width (G), and array periodicity (P), as illustrated in Figure 2a. The cutoff wavelength of a coaxial aperture made with a perfect electrical conductor is given by $\lambda_c = n\pi (R_o + R_i)$, where n is the refractive index of the insulator and R_o and R_i are the radius of the outer and inner surfaces of the gap, respectively.[9] For coaxial apertures made with a real metal, however, the cutoff wavelength can differ dramatically from this PEC approximation, especially as the gap size is reduced.[9] To prove our coaxial waveguides exhibit singular optical behavior, we experimentally measured the optical transmission spectra through coaxial aperture arrays with a 250 nm inner diameter and four different gap widths (2, 4, 7, 10 nm). Spectra were collected using a Si CCD, InGaAs photodiode array, and FTIR spectrometer, respectively, in the visible, NIR, and mid-infrared (MIR) regions (Figure 2d). Multiple peaks for a given gap size are observed throughout the entire spectrum. The most notable feature of the measured spectra is the presence of intense MIR EOT peaks. For a 10 nm gap size and inner diameter of 250 nm, the strongest resonance peak occurs at the free-space wavelength of 2800 nm with an aperture-normalized transmission of 1170%. Table 1 shows the aperture-normalized and

Table 1. EOT Calculated from the Measured Transmission with Different Gap Widths

gap width (nm)	measured transmission (%)	open area fraction (%)	area-normalized transmission (%)
10	36	3.06	1170
7	25	2.28	1090
4	15	1.35	1120
2	12	0.69	1740

absolute transmission from different gap sizes. Interestingly, as the gap size shrinks, the resonance wavelength of the EOT increases dramatically (Figure 2d,e).

When first described, EOT initially referred to transmission greater than unity through periodic metallic apertures in cutoff, that is, the field inside the aperture is evanescent. In that case, the incoming electromagnetic field couples to surface plasmons of the corrugated surface of a metal film, trapping energy in the system for an extended time leading to increased tunneling through the apertures. This definition has since been expanded to include optical resonances that lead to enhanced transmission in general, irrespective of whether the individual

apertures are in cutoff, and a nonexhaustive list now includes cutoff resonances, Brewster-like resonances, and absorption-induced transparency.[32] In our coaxial aperture array, the periodicity of 500 nm was chosen to confine surface resonance effects to the NIR (900 nm), thereby ensuring the observed MIR peaks are not due to surface resonances or a periodic effect. Instead, enhanced transmission in our coaxial waveguides is induced by Fabry-Pérot (FP) type resonances that propagate along the length of the aperture. Notably, there is a special zeroth-order FP case, which occurs spectrally close to the cutoff frequency of the TE_{11} waveguide mode, where EOT can arise as well.

The multiple peaks for a given gap size in our devices emerge from these series of FP modes, including the zeroth-order cutoff resonance, and span over a full octave in frequency. The lowest-frequency peak we observe in the MIR should correspond to the zeroth-order cutoff resonance, and the next resonance peak in the NIR corresponds to a first-order FP mode. In the first-order FP mode, light traveling in the Al_2O_3-filled coaxial MIM waveguide is partially reflected at the upper and lower surfaces of the metal film, forming a resonator whose cavity length (L) is equal to the film thickness, provided that the following condition is satisfied

$$|2L\beta + \Delta\phi_1 + \Delta\phi_2| = 2\pi m \tag{1}$$

where β is the propagation constant in the MIM coaxial waveguide, $m \geq 0$ is the integer representing the mode number ($m = 1$ in this case), and $\Delta\phi_{1,2}$ are the phase shifts due to reflection.[10] As alluded to earlier, $m = 0$ is a valid solution to the FP condition as well, so long as $\beta \to 0$, which explains why the cutoff resonance can be described using FP nomenclature.

The physical origin of the observed peaks is further analyzed by comparing the measured data to computer simulations. Because of the large-scale mismatch in the wavelength (up to 6 μm) and gap size (<10 nm), we chose an advanced finite-element method based on a hybridizable discontinuous Galerkin (HDG) scheme, which is optimized to handle such multiscale problems.[20] In this work, the HDG method is used to solve the time-harmonic Maxwell's equations on an anisotropic unstructured mesh of 21 384 quartic hexagonal elements. The accuracy of these results is verified by performing a grid convergence study in which we carry out the simulations on three consecutively refined meshes and observe that the difference in the maximum EOT between the medium mesh and the fine mesh is less than 0.25% for all cases. The calculated EOT spectra (Figure 2d) agree well with the measured spectra for a 10 nm gap coaxial aperture array. For gap sizes below 4 nm, the mismatch increases likely due to fabrication imperfections such as roughness of the interior metal surfaces. In the size regime presented, even subnanometer changes in the gap width can have large effects on the position of resonant peaks. Additionally, the realistic bulk dielectric constant values for an ALD-grown Al_2O_3 thin film used in simulation can diverge from experimental values for narrower gaps (below 4 nm). The calculated electric field maps for two observed peaks are plotted in Figure 2g. For illumination at normal incidence using linearly polarized light, the fundamental TEM mode of a coaxial waveguide cannot be excited due to the mismatch in mode symmetry, but higher-order modes with nonzero angular momentum can. The field profiles of the cross-section atop the coaxial aperture show that the transmission resonances arise from TE_{11} modes (the lowest order mode with nonzero angular momentum). At the ENZ
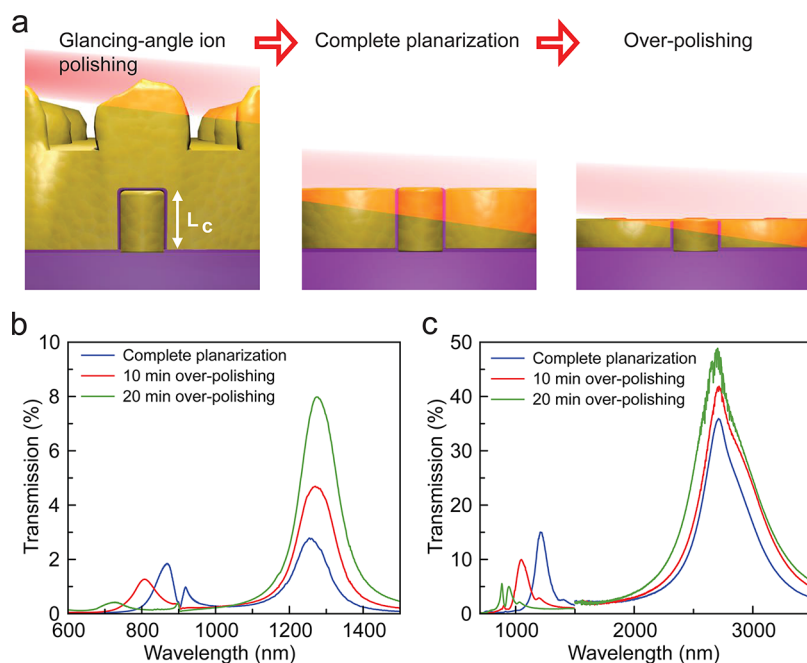
Figure 3. Experimental verification of the FP0 cutoff resonance mode by the dispersion properties of the resonant peaks. (a) Schematic of glancing-angle ion polishing to reduce the cavity length. (b,c) The change in the transmitted spectra as glancing-angle ion polishing time increases and film thickness decreases from a coaxial aperture array with a 10 nm gap width and diameters of 100 and 250 nm, respectively.
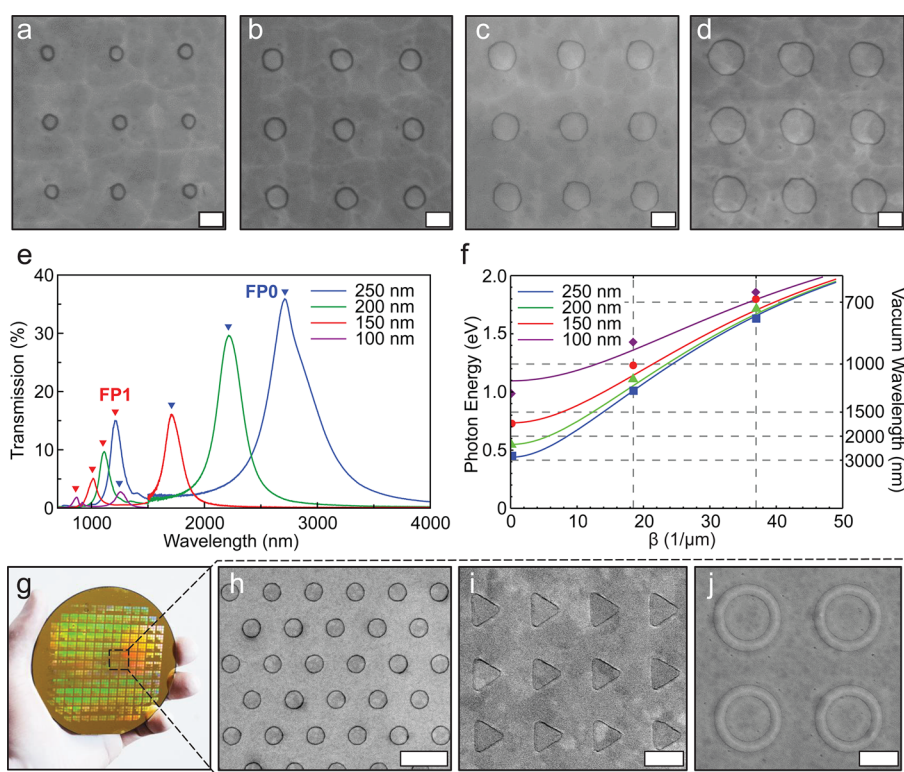

Figure 4. Effect of diameter on the transmission resonances excited in a coaxial aperture array. (a−d) SEM images of coaxial aperture arrays with 100, 150, 200, and 250 nm diameters, respectively. (e) The transmitted spectra from the coaxial 10 nm gap with 100, 150, 200, 250 nm diameters. (f) The dispersion curve of the plasmonic coaxial aperture. FP0 ($m = 0$), FP1 ($m = 1$), and FP2 ($m = 2$) resonances (experimental data) are fitted with the analytical dispersion curve. (g) Photograph of a 4-in. wafer fully patterned with dense arrays of nanocavities with various shapes. Zoomed-in SEM images of wafer-scale arrays of (h) coaxial nanocavities, (i) triangular nanocavities, and (j) concentric annular nanocavities. These arrays were patterned via photolithography. Scale bars: (a−d) 150 nm, (h−j) 1 μm.

condition, the phase velocity is so large that the phase shift between the entrance and exit sides of the coaxial waveguide becomes very small, leading to uniform electric fields inside the nanogap as shown in the vertically cross-cut field map corresponding to the MIR resonance. The simulation results also indicate that this is indeed a cutoff resonance (FP0 mode).

The resulting slow light effect can enable extremely strong field intensity enhancements (over 6000 observed in simulation) inside the ultrasmall coaxial nanocavities as the gap size narrows to only 2 nm (Figure 2f).

We studied the dispersion properties of these peaks experimentally by shortening the FP cavity length. This was accomplished by continuing the glancing-angle ion polishing past planarization (Figure 3a). As the cavity length is reduced, the resonance wavelength of the FP0 mode, which is determined by the cutoff frequency and has a propagation constant of practically zero, does not change appreciably while the FP1 peak blue shifts (Figure 3b,c). We note that there is a small reflection phase that at resonance has to be canceled with an "optical path" phase, slightly shifting the resonance away from the cutoff frequency. This is important for very thin metal films[33] but not for the thicknesses considered in this work. The film-thickness-independent property of the FP0 mode also explains the nature of previously observed terahertz resonances alongside millimeter-scale loops in earlier work,[19] which was not explicitly mentioned. In that case, the film thickness was only 150 nm whereas the resonance wavelength was in the millimeter-scale, thus FP1 or higher-order modes could not be sustained in the thin film, while FP0 resonances were still present. This property of the FP0 "slow light" mode, which is independent of the length of the waveguide, exhibits ENZ behavior. In addition, the resonator periodicity can be much smaller than the resonance wavelength as demonstrated, and thus our coaxial resonator array can be a practical platform to construct large-area ENZ metamaterials.

The TE_{11} resonances of our devices can be tuned by changing the aperture diameter. The propagation constant β, transverse wavevector $\mathbf{k}_\theta$ of a coaxial aperture waveguide, and the propagation constant β_{MIM} of a planar MIM waveguide, should satisfy the following condition[11]

$$\beta^2 + \mathbf{k}_\theta^2 = \beta_{MIM}^2 \qquad (2)$$

$$2\pi R \mathbf{k}_\theta = 2\pi\nu \qquad (3)$$

where ν is an integer and R is the average radius. The cutoff frequency is thus influenced by the diameter of the coaxial aperture. To investigate this effect, coaxial apertures with a 10 nm gap were fabricated with ring diameters of 100, 150, 200, and 250 nm (Figure 4a–d). As shown in Figure 4e, the FP0 resonance peak blue shifts with a decreasing diameter, as expected. These properties of FP resonances as a function of the aperture diameter can be explained by the theoretical dispersion calculated from eq 3.[11] The dispersions of coaxial MIM structure are plotted using eqs 2 and 3 and compared with experimental data in Figure 4f. A unique feature of coaxial apertures is that this cutoff wavelength decreases along with the aperture diameter while maintaining the gap size and hence the field confinement. Thus, a simple coaxial aperture geometry can be used to create extreme subwavelength resonators covering visible, IR, and terahertz frequencies. These effects are characteristic of an individual coaxial waveguide, rather than a periodic effect, as the change in the periodicity does not shift FP0 frequencies (Figure S3). Furthermore, the cutoff resonance frequencies for these FP0 modes do not change with the incident angle of illumination, as confirmed by theoretical modeling (Figure S4), making these structures ideal for applications where angle independence is important.[34,35] Reserved for future work, FP0 modes in the visible are achievable even with 10 nm gaps by reducing the aperture

diameter to 40–50 nm (Figure S5). Using our new fabrication scheme, these coaxial nanocavities featuring unique optical properties can now be fabricated over an entire 4 in. wafer when combined with nanoimprint or photolithography (Figure 4g–i).

In summary, we have combined atomic layer lithography and wafer-scale glancing-angle ion polishing to manufacture ENZ metamaterials consisting of single-digit-nanometer-gap coaxial resonators and investigated their characteristic EOT and slow-light properties. These results demonstrated a 100-fold improvement in device characteristics over our previous work by decreasing the individual resonator footprint from tens of micrometers to ~100 nm, enabling the exploration of EOT as well as ENZ properties in the infrared regimes. Unlike multilayer film stacks for ENZ, our coaxial aperture array can be made at wafer scale and readily couple normally incident light independent of polarization, making this a practical ENZ platform utilizing EOT. Our choice of 500 nm array periodicity confines periodic coupling effects to the NIR regime while sub-10 nm gap widths push the FP1 and FP0 resonances of an individual coaxial aperture toward the MIR, allowing unambiguous observations of these properties and proving that the observed resonances arise from the properties of individual apertures. The gap width is as small as $\lambda/1900$ at MIR resonances, and the cutoff resonance wavelength of each resonator (2–4 μm) is much larger than its unit cell size (cavity diameter of ~250 nm). Additionally, the volume of the Al_2O_3-filled gap is as small as $\lambda^3/10^6$ for MIR operation, making these structures one of the smallest nanophotonic resonators to date. Our high-throughput fabrication technique can be applied to a wide range of metals and gap-filling insulators as well as for resonators in the visible regime and with different shapes. The metal pillars and surrounding film can be addressed as electrodes, potentially allowing for the electrical generation of plasmons by tunneling directly in the waveguides.[36−39] Furthermore, the intense fields of this extremely confined slow-light mode at the ENZ condition can be accessed from the flat top surface and coupled with other materials for applications in biosensing,[40,41] surface-enhanced spectroscopies,[42−46] optical trapping,[30,47] and nonlinear optics.[23,48,49] Our work demonstrates that metamaterials with extreme subwavelength features such as single-digit-nanometer gaps can now be manufactured for practical applications.

■ ASSOCIATED CONTENT

Ⓢ Supporting Information

The Supporting Information is available free of charge on the ACS Publications website at DOI: 10.1021/acs.nanolett.6b00024.

> Methods for device fabrication, optical measurements, and computer simulations for the angular and periodic dependences on the transmission resonances of coaxial aperture arrays. (PDF)
> CFDTD movie of the FP0 mode in a resonances of coaxial aperture array. (MPG)

■ AUTHOR INFORMATION

Corresponding Author
*E-mail: sang@umn.edu.

Author Contributions

D.Y. and S.-H.O. conceived and designed the experiments. D.Y. performed sample fabrication and electron microscopy. N.C.N.,

■ **REFERENCES**

(1) Ebbesen, T. W.; Lezec, H. J.; Ghaemi, H. F.; Thio, T.; Wolff, P. A. *Nature* **1998**, *391*, 667−669.

(2) Martín-Moreno, L.; García-Vidal, F. J.; Lezec, H. J.; Pellerin, K. M.; Thio, T.; Pendry, J. B.; Ebbesen, T. W. *Phys. Rev. Lett.* **2001**, *86*, 1114−1117.

(3) Brolo, A. G.; Gordon, R.; Leathem, B.; Kavanagh, K. L. *Langmuir* **2004**, *20*, 4813−4815.

(4) Miyazaki, H. T.; Kurokawa, Y. *Phys. Rev. Lett.* **2006**, *96*, 097401.

(5) Bozhevolnyi, S. I.; Volkov, V. S.; Devaux, E.; Laluet, J.-Y.; Ebbesen, T. W. *Nature* **2006**, *440*, 508−511.

(6) Halas, N. J. *Nano Lett.* **2010**, *10*, 3816−3822.

(7) Baida, F. I.; Van Labeke, D. *Opt. Commun.* **2002**, *209*, 17−22.

(8) Orbons, S. M.; Roberts, A. *Opt. Express* **2006**, *14*, 12623−12628.

(9) Baida, F. I.; Belkhir, A.; Van Labeke, D.; Lamrous, O. *Phys. Rev. B: Condens. Matter Mater. Phys.* **2006**, *74*, 205419.

(10) de Waele, R.; Burgos, S. P.; Polman, A.; Atwater, H. A. *Nano Lett.* **2009**, *9*, 2832−2837.

(11) Catrysse, P. B.; Fan, S. *Appl. Phys. Lett.* **2009**, *94*, 231111.

(12) García-Vidal, F. J.; Martín-Moreno, L.; Ebbesen, T. W.; Kuipers, L. *Rev. Mod. Phys.* **2010**, *82*, 729−787.

(13) Edwards, B.; Alù, A.; Young, M. E.; Silveirinha, M.; Engheta, N. *Phys. Rev. Lett.* **2008**, *100*, 033903.

(14) Maas, R.; Parsons, J.; Engheta, N.; Polman, A. *Nat. Photonics* **2013**, *7*, 907−912.

(15) Silveirinha, M. G.; Engheta, N. *Phys. Rev. B: Condens. Matter Mater. Phys.* **2007**, *76*, 245109.

(16) Fan, W.; Zhang, S.; Minhas, B.; Malloy, K. J.; Brueck, S. R. J. *Phys. Rev. Lett.* **2005**, *94*, 033902.

(17) Fan, W.; Zhang, S.; Malloy, K. J.; Brueck, S. R. J. *Opt. Express* **2005**, *13*, 4406−4413.

(18) Melli, M.; Polyakov, A.; Gargas, D.; Huynh, C.; Scipioni, L.; Bao, W.; Ogletree, D. F.; Schuck, P. J.; Cabrini, S.; Weber-Bargioni, A. *Nano Lett.* **2013**, *13*, 2687−2691.

(19) Chen, X.; Park, H.-R.; Pelton, M.; Piao, X.; Lindquist, N. C.; Im, H.; Kim, Y. J.; Ahn, J. S.; Ahn, K. J.; Park, N.; Kim, D.-S.; Oh, S.-H. *Nat. Commun.* **2013**, *4*, 2361.

(20) Park, H.-R.; Chen, X.; Nguyen, N.-C.; Peraire, J.; Oh, S.-H. *ACS Photonics* **2015**, *2*, 417−424.

(21) George, S. M. *Chem. Rev.* **2010**, *110*, 111−131.

(22) Lindquist, N. C.; Nagpal, P.; McPeak, K. M.; Norris, D. J.; Oh, S.-H. *Rep. Prog. Phys.* **2012**, *75*, 036501.

(23) Fan, W.; Zhang, S.; Panoiu, N.-C.; Abdenour, A.; Krishna, S.; Osgood, R. M.; Malloy, K. J.; Brueck, S. R. J. *Nano Lett.* **2006**, *6*, 1027−1030.

(24) Argyropoulos, C.; Chen, P.-Y.; D'Aguanno, G.; Engheta, N. *Phys. Rev. B: Condens. Matter Mater. Phys.* **2012**, *85*, 045129.

(25) Burgos, S. P.; de Waele, R.; Polman, A.; Atwater, H. A. *Nat. Mater.* **2010**, *9*, 407−412.

(26) van de Haar, M. A.; Maas, R.; Schokker, H.; Polman, A. *Nano Lett.* **2014**, *14*, 6356−6360.

(27) Tsakmakidis, K. L.; Boardman, A. D.; Hess, O. *Nature* **2007**, *450*, 397−401.

(28) Atwater, H. A.; Polman, A. *Nat. Mater.* **2010**, *9*, 205−213.

(29) Khajavikhan, M.; Simic, A.; Katz, M.; Lee, J. H.; Slutsky, B.; Mizrahi, A.; Lomakin, V.; Fainman, Y. *Nature* **2012**, *482*, 204−207.

(30) Saleh, A. A. E.; Dionne, J. A. *Nano Lett.* **2012**, *12*, 5581−5586.

(31) Alù, A.; Engheta, N. *Phys. Rev. Lett.* **2009**, *103*, 043902.

(32) Hutchison, J. A.; O'Carroll, D. M.; Schwartz, T.; Genet, C.; Ebbesen, T. W. *Angew. Chem., Int. Ed.* **2011**, *50*, 2085−2089.

(33) Carretero-Palacios, S.; García-Vidal, F. J.; Martín-Moreno, L.; Rodrigo, S. G. *Phys. Rev. B: Condens. Matter Mater. Phys.* **2012**, *85*, 035417.

(34) Lockyear, M. J.; Hibbins, A. P.; Sambles, J. R.; Lawrence, C. R. *Phys. Rev. Lett.* **2005**, *94*, 193902.

(35) Baida, F. I. *Appl. Phys. B: Lasers Opt.* **2007**, *89*, 145−149.

(36) Lambe, J.; McCarthy, S. L. *Phys. Rev. Lett.* **1976**, *37*, 923−925.

(37) Esteban, R.; Borisov, A. G.; Nordlander, P.; Aizpurua, J. *Nat. Commun.* **2012**, *3*, 825.

(38) Parzefall, M.; Bharadwaj, P.; Jain, A.; Taniguchi, T.; Watanabe, K.; Novotny, L. *Nat. Nanotechnol.* **2015**, *10*, 1058−1063.

(39) Marinica, D. C.; Zapata, M.; Nordlander, P.; Kazansky, A. K.; Echenique, P. M.; Aizpurua, J.; Borisov, A. G. *Science Advances* **2015**, *1*, e1501095.

(40) Lal, S.; Link, S.; Halas, N. J. *Nat. Photonics* **2007**, *1*, 641−648.

(41) Gordon, R.; Sinton, D.; Kavanagh, K. L.; Brolo, A. G. *Acc. Chem. Res.* **2008**, *41*, 1049−1057.

(42) Xu, H.; Bjerneld, E. J.; Käll, M.; Börjesson, L. *Phys. Rev. Lett.* **1999**, *83*, 4357−4360.

(43) Ward, D. R.; Grady, N. K.; Levin, C. S.; Halas, N. J.; Wu, Y.; Nordlander, P.; Natelson, D. *Nano Lett.* **2007**, *7*, 1396−1400.

(44) Im, H.; Bantz, K. C.; Lindquist, N. C.; Haynes, C. L.; Oh, S.-H. *Nano Lett.* **2010**, *10*, 2231−2236.

(45) Brown, L. V.; Zhao, K.; King, N.; Sobhani, H.; Nordlander, P.; Halas, N. J. *J. Am. Chem. Soc.* **2013**, *135*, 3688−3695.

(46) Chen, X.; Ciracì, C.; Smith, D. R.; Oh, S.-H. *Nano Lett.* **2015**, *15*, 107−113.

(47) Pang, Y.; Gordon, R. *Nano Lett.* **2012**, *12*, 402−406.

(48) Kauranen, M.; Zayats, A. V. *Nat. Photonics* **2012**, *6*, 737−748.

(49) Lassiter, J. B.; Chen, X.; Liu, X.; Ciracì, C.; Hoang, T. B.; Larouche, S.; Oh, S.-H.; Mikkelsen, M. H.; Smith, D. R. *ACS Photonics* **2014**, *1*, 1212−1217.